Original Article

Institution of MECHANICAL ENGINEERS
Journal of MECHANICAL ENGINEERING SCIENCE

Proc IMechE Part C:
J Mechanical Engineering Science
2016, Vol. 230(19) 3431–3441

DOI: 10.1177/0954406215612829
pic.sagepub.com
SAGE

# Heat transfer characteristics of slip flow over solid spheres

**Morteza Anbarsooz[1] and Hamid Niazmand[2]**

**Abstract**

In this study, heat transfer characteristics of slip flow over an isolated impermeable solid sphere are investigated numerically. An isothermal solid sphere is considered at intermediate Reynolds numbers ($0 \leqslant Re \leqslant 50$) for Prandtl numbers in the range of 0.7–7.0. The Navier–Stokes and energy equations are solved by a control volume technique in conjunction with the velocity slip and temperature jump boundary conditions. It was found that the size of the thermal wake region according to the Knudsen number depends on the Prandtl number. At lower Prandtl numbers ($0.7 \leqslant Pr \leqslant 2.0$), the thermal wake region shrinks as the Knudsen number increases, while at higher Prandtl numbers, it grows as the Knudsen number increases. The maximum temperature jump occurs at the front stagnation point where the local Nusselt is itself maximum, owing to the maximum temperature gradient at this point. The results show that due to the opposing effects of the velocity slip and temperature jump, the average Nusselt number variation with the Knudsen number depends nonlinearly on both the Prandtl and Reynolds numbers. Furthermore, for the limiting case of $Re \to 0$, an analytical solution for the problem is presented which has also served as a validation case.

**Keywords**

Slip flow, temperature jump, thermal wake, Nusselt number

Date received: 30 November 2014; accepted: 22 September 2015

## Introduction

Fluid flow and especially heat and mass transfer from spheres are essential issues in many engineering and environmental applications such as spray drying, extraction, humidification, aerosol scrubbing and evaporation, and fuel droplets heating and evaporation, among others.

The classical problem of heat transfer from a sphere has been the subject of several investigations in the past. Heat transfer from spheres is governed by two independent dimensionless parameters, the Reynolds number and the Peclet number, which account for the velocity and temperature fields, respectively. The available solutions for the flow and temperature fields over spheres can be classified based on the Reynolds number. At creeping flow regime (Reynolds numbers less than one), analytical solution of viscous flow over spherical particles exist for both rigid spheres[1,2] and liquid spheres.[3,4] At Reynolds numbers higher than one, however, stream function form of the momentum equations have been solved numerically for flow over solid spheres.[5–13] A solution of the transient heat transfer from a solid sphere at creeping flow regime is presented by Carslaw and Jaeger.[14] Also, an analytical expression for the heat transfer from a small spherical particle can be found in Feng and Michaelides[15] at low Peclet numbers assuming a Stokesian velocity distribution around the sphere. Solutions to the stream function form of the heat or mass transfer equation have also been obtained by many researchers using the finite-difference schemes.[11,16–19]

In all of the above mentioned studies, the boundary condition applied to the solid sphere surface is the well-known no-slip condition. This boundary condition, however, can be violated in many practical applications, which can be classified into two main categories:

(a) Slip flow regime,[20] where the sphere diameter is comparable with the mean free path of its

[1]Mechanical Engineering Department, Quchan University of Advanced Technology, Quchan, Iran
[2]Mechanical Engineering Department, Ferdowsi University of Mashhad, Mashhad, Iran

**Corresponding author:**
Morteza Anbarsooz, Mechanical Engineering Department, Quchan University of Advanced Technology, Quchan 94771-67335, Iran.
Email: anbarsouz@qiet.ac.ir

surrounding gas molecules and some degrees of rarefaction effects are present.

(b) Liquid flow over hydrophobic surfaces,[21] where slip occurs as a surface phenomenon due to the surface properties of the solid.

Despite the differences in fundamental physics associated with each category, they both can be treated similarly in numerical modeling under a unified boundary condition. In this regard, incompressible flow simulations with appropriate slip boundary conditions have been employed by various researchers for both categories, yet the presentation of the boundary conditions is slightly different. As a result, it seems reasonable to make an attempt in developing a unified boundary condition applicable to both categories, which has not been addressed in previous studies. What follows is a review on main characteristics of each category and the related literature.

In the first category, the so called *"slip flow regime"*, fluid slippage on walls occurs due to fluid rarefaction effects. The degree of rarefaction is evaluated via Knudsen number defined as the ratio of the mean free path of the surrounding gas molecules, $\lambda$, to the diameter of the spherical particle, $D$. It is well established that the medium is continuous for $\mathrm{Kn} \leqslant 10^{-3}$, and Navier–Stokes equations with the no-slip boundary condition on walls predict the flow field accurately.[20] On the other hand, for $\mathrm{Kn} > 10$ the continuum approach breaks down completely and a free molecular flow is developed. However, for $0.001 \leqslant \mathrm{Kn} \leqslant 0.1$, which is commonly referred to as the slip flow regime, slight rarefaction effects are present and the Navier–Stokes equations can still be employed in conjunction with modified boundary conditions known as velocity slip and temperature jump at walls.[20]

In many industrial applications where micron-sized particles interact with a gas such as air at atmospheric pressures ($\lambda = 70$ nanometer), the associated particle Knudsen number lies in the slip flow regime. The particles Reynolds numbers, however, are commonly in the Stokes flow regime due to their micron size diameters. Yet, in many applications particles, Reynolds numbers can reach values much higher than those of the creeping flow regime.[22,23] There have been several studies related to the spheres in the rarefied gas flows. However, most of them have focused on experimentally determining the particles drag coefficient in Stokes' flow regime by introducing correction factors.[24–30] Recently, numerical studies on rarefaction effects on the sphere drag coefficient have been performed in Stokes' flow regime[31] and also at intermediate Reynolds numbers.[32,33] However, not much information is available related to the heat transfer characteristics of spheres in the slip flow regime.

Nevertheless, numerous investigations have been performed to study the fluid flow and heat transfer behavior in micro-scale devices such as the micro-channels. Some of these studies are performed on gaseous flows in slip flow regime over curved surfaces in which the physical curved space is mapped to a uniform computational space. Effects of Knudsen number, geometry, creep flow, viscous dissipation, etc. have been investigated.[34–37]

In the second category, the liquid slips on walls because of the solid surface hydrophobic interaction and it is characterized by the Trostel number defined as[38]

$$\mathrm{Tr} = \frac{\lambda' D}{\mu} \tag{1}$$

where $\mu$ is the liquid viscosity and $\lambda'$ is a positive scalar varying from zero to infinity, which is a function of liquid and wall properties, surface temperature, and wall roughness. At no-slip condition, the Trostel number is infinite and in full-slip condition is equal to zero. Watanabe et al.[21,39–41] produced the pioneering researches on slip of Newtonian liquids on walls in macro-scale. They computed the slip coefficient of different surfaces experimentally, showing that shear stress is proportional to liquid slip-velocity on walls. Atefi et al.[38] have numerically studied the fluid dynamics of slip flow over hydrophobic solid spheres at intermediate Reynolds numbers.

Despite the rich literature on the fluid dynamics of slip flow over solid spheres in both categories as reviewed above, no considerable investigations have ever been made on the heat transfer characteristics of slip flow over spheres. The current paper, however, focuses on heat transfer characteristics of slip flow over solid spheres. Momentum and energy equations are solved numerically for an incompressible flow over an isothermal solid sphere using the velocity–slip and temperature jump boundary conditions on wall at Reynolds numbers of $0 \leqslant \mathrm{Re} \leqslant 50$ for $0.7 \leqslant \mathrm{Pr} \leqslant 7.0$. The boundary conditions are unified in a manner that can be employed in both flow categories. The numerical results are presented in terms of Knudsen number, which is directly related to Trostel number as will be given later. Temperature contours, thermal wake structure, temperature jump and local Nusselt number distributions have been examined in detail. In addition, an analytical solution for the $\mathrm{Re} \to 0$ limit is developed which can also serve as a validation case for the presented numerical results.

## Numerical procedure

### Governing equations

A schematic diagram of the problem and the coordinate system is presented in Figure 1. A uniform flow in the $x$-direction with the initial temperature of $T_\infty$ passes over an impermeable isothermal solid sphere at $T_w$. According to the range of Reynolds numbers considered here ($0 \leqslant \mathrm{Re} \leqslant 50$), the problem will remain axisymmetric. Continuity, momentum, and energy equations for the laminar incompressible flow of a

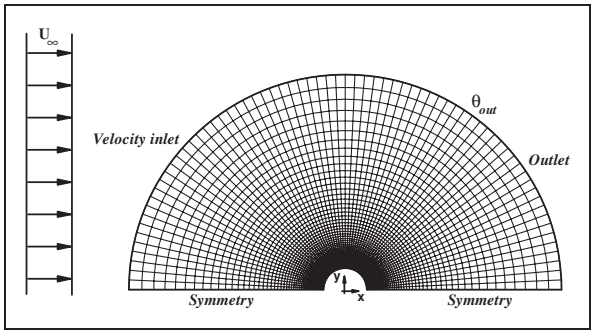


**Figure 1.** A schematic of the problem, computational grid and the boundary conditions.

Newtonian fluid with constant properties in the spherical coordinates $(r, \varphi)$ are as follows

$$\frac{1}{r^2}\frac{\partial}{\partial r}\left(r^2 v_r\right) + \frac{1}{r\sin\varphi}\frac{\partial}{\partial \varphi}\left(v_\varphi \sin\varphi\right) = 0 \tag{2}$$

$$\begin{aligned}&\frac{\partial v_r}{\partial t} + v_r\frac{\partial v_r}{\partial r} + \frac{v_\varphi}{r}\frac{\partial v_r}{\partial \varphi} - \frac{v_\varphi^2}{r}\\ &\quad = -\frac{\partial p}{\partial r} + \frac{1}{\mathrm{Re}}\left(\frac{\partial}{\partial r}\left(\frac{1}{r^2}\frac{\partial}{\partial r}\left(r^2 v_r\right)\right) + \frac{1}{r^2\sin\varphi}\frac{\partial}{\partial \varphi}\right.\\ &\qquad \left.\times\left(\sin\varphi\frac{\partial v_r}{\partial \varphi}\right) - \frac{2}{r^2\sin\varphi}\frac{\partial}{\partial \varphi}\left(v_\varphi\sin\varphi\right)\right)\end{aligned} \tag{3}$$

$$\begin{aligned}&\frac{\partial v_\varphi}{\partial t} + v_r\frac{\partial v_\varphi}{\partial r} + \frac{v_\varphi}{r}\frac{\partial v_\varphi}{\partial \varphi} + \frac{v_r v_\varphi}{r}\\ &\quad = -\frac{\partial p}{\partial \varphi} + \frac{1}{\mathrm{Re}}\left(\frac{1}{r^2}\frac{\partial}{\partial r}\left(r^2\frac{\partial v_\varphi}{\partial r}\right) + \frac{1}{r^2}\frac{\partial}{\partial \varphi}\right.\\ &\qquad \left.\times\left(\frac{1}{\sin\varphi}\frac{\partial}{\partial \varphi}\left(v_\varphi\sin\varphi\right)\right) + \frac{2}{r^2}\frac{\partial v_r}{\partial \varphi}\right)\end{aligned} \tag{4}$$

$$\begin{aligned}&\frac{\partial \theta}{\partial t} + v_r\frac{\partial \theta}{\partial r} + \frac{v_\varphi}{r}\frac{\partial \theta}{\partial \varphi}\\ &= \frac{1}{\mathrm{Re}\,\mathrm{Pr}}\left(\frac{1}{r^2}\frac{\partial}{\partial r}\left(r^2\frac{\partial \theta}{\partial r}\right) + \frac{1}{r^2\sin\varphi}\frac{\partial}{\partial \varphi}\left(\sin\varphi\frac{\partial \theta}{\partial \varphi}\right)\right)\end{aligned} \tag{5}$$

All the variables in the above equations are non-dimensional; $v_r$ and $v_\theta$ are the dimensionless velocity components in the radial and tangential directions, respectively; $\theta = (T - T_\infty)/(T_w - T_\infty)$, the non-dimensional temperature; $T_w$, the wall temperature and $T_\infty$ is the free stream temperature. $\rho_\infty$, $U_\infty$ and $\rho_\infty U_\infty^2$ are used as the reference density, velocity and pressure, respectively. Re is Reynolds number defined as $\mathrm{Re} = \rho U_\infty D/\mu$, Pr is the Prandtl number, $\mu$ is the gas viscosity, $D$ is the sphere diameter, $\rho$, the density, $p$, the pressure, and $\mu$ the gas viscosity.[42]

## Computational grid and boundary conditions

The computational grid system and the boundary conditions are also shown in Figure 1. The grid distribution close to the sphere surface is refined in the radial direction to resolve high gradients in this region. The outer boundary is divided into inflow and outflow sections by $\theta_{out}$, and its location should be adjusted according to the flow Reynolds number. Present numerical investigations indicate that 120° from the front stagnation point for $\theta_{out}$ works well for all Reynolds numbers above 1, while for lower Re it should be moved towards the 90° angle.[42,43] For the outlet section, all gradients are set to zero in the radial direction, while uniform flow is specified for the inlet section. Symmetrical conditions are applied on the horizontal axis.

On walls, the conventional no-slip boundary condition must be replaced by appropriate slip velocity. However, as stated in the introduction section, the presentation of the boundary conditions is slightly different in the two mentioned categories. For the first category that is the slip flow regime, the first-order slip velocity for an ideal gas has been expressed by Maxwell[44] as

$$u_s - u_w = \left(\frac{2-\sigma_v}{\sigma_v}\right)\mathrm{Kn}\frac{\partial u_s}{\partial n} \tag{6}$$

where $u_s$ and $u_w$ are the non-dimensional tangential slip and wall velocities, respectively; $n$ is the wall normal direction and $\sigma_v$ is the tangential momentum accommodation factor, which describes the interaction of gas molecules with the wall.[20] For the second category, however, the boundary condition proposed by Trostel[45] for a general case of flow slippage on a solid surface is

$$u_s - u_w = \frac{1}{\mathrm{Tr}}\frac{\partial u_s}{\partial n} \tag{7}$$

Comparing these two boundary conditions reveals that despite the complete difference in the governing physics of these two flow categories, they have been both treated similarly in numerical modeling. Therefore, the numerical results obtained based on one of these boundary conditions can be used in the other flow category using the following relation

$$\mathrm{Tr} = \frac{\sigma_v}{2-\sigma_v}\frac{1}{\mathrm{Kn}} \tag{8}$$

Likewise, the temperature continuity at the wall must be replaced by appropriate temperature jump boundary condition. For the slip flow regime, Smoluchowski von Smolan[46] represented the first-order temperature jump boundary condition as follows

$$T_g - T_w = \left(\frac{2\gamma}{\gamma+1}\right)\left(\frac{2-\sigma_T}{\sigma_T}\right)\left(\frac{\mathrm{Kn}}{\mathrm{Pr}}\right)\left(\frac{\partial T}{\partial n}\right) \tag{9}$$

where $T_w$ is the dimensionless wall temperature, $T_g$ the dimensionless temperature of the first layer of

gas adjacent to the wall, $\gamma$ the gas specific heat capacity ratio, $\sigma_T$ the thermal accommodation coefficient, Pr the Prandtl number, and $\partial T/\partial n$ is the normal temperature gradient at the wall. Generally, the values of the tangential momentum and thermal accommodation coefficients depend on the surface finish and velocity at the fluid–wall interface, which are commonly determined experimentally. They vary from nearly zero to unity for specular and diffuse reflections, respectively. For most engineering applications, the value of accommodation coefficients is close to unity[20] and considering the approximate nature of the slip velocity formulation, they are both taken as unity in the present study.

For the second category, no investigation has ever been made on the heat transfer characteristics and therefore no boundary condition is available in the literature. Inspired by the similarity between slip–velocity treatments in the both flow categories discussed above, it is assumed that the temperature jump boundary condition in the second flow category is also proportional to the normal temperature gradient, as it is in the slip flow regime.

In this study, all numerical simulations are performed based on the boundary conditions proposed for the slip flow regime that are equations (6) and (9) for fluid flow and heat transfer equations, respectively. However, for liquid flow over hydrophobic surfaces, the corresponding Tr number must be calculated first using equation (8).

### Solution procedure

The numerical solution is based on a projection-type method, which has been self-coded. This numerical scheme is originally developed by Chorin,[47] and improved further by Dwyer[43] and the present authors.[48] The principle of the numerical method is based upon the calculation of an intermediate velocity field, $\vec{V}^*$, from momentum equations using the pressure field from previous time step

$$\frac{\vec{V}^* - \vec{V}^n}{\Delta t} + \nabla \cdot \left(\vec{V}^n \vec{V}^*\right) = -\nabla p^n + \frac{1}{\mathrm{Re}} \nabla^2 \vec{V}^* \qquad (10)$$

This intermediate velocity field does not necessarily satisfy the mass conservation equation and thus a velocity correction is introduced. According to the Hodge decomposition theorem, which states that any vector function can be decomposed into a divergence-free component and the gradient of a scalar potential, a velocity potential is assigned to the velocity correction. This is consistent with the fact that an intermediate velocity field obtained from the momentum equations using an existing pressure field carries the exact vorticity information, and therefore, the velocity correction comes from an irrotational field that can be described with a velocity potential. As a result, the velocity and pressure corrections can be expressed as

$$\frac{\vec{V}^{n+1} - \vec{V}^*}{\Delta t} = -\nabla \alpha \qquad (11)$$

$$P^{n+1} = P^n + \alpha \qquad (12)$$

The velocity field in the new time step, $\vec{V}^{n+1}$, has to satisfy the continuity equation, $\vec{\nabla} \cdot \vec{V}^{n+1} = 0$. Therefore, the pressure correction could be determined from the following relation using the known intermediate velocity field

$$\nabla^2 \alpha = \frac{1}{\Delta t} \vec{\nabla} \cdot \vec{V}^* \qquad (13)$$

## Mesh study and validations

Grid-independency studies are performed by comparing the total drag coefficient and the average Nusselt number for six different grid resolutions at $\mathrm{Re} = 30$ and $\mathrm{Pr} = 1.0$ in the no slip regime as tabulated in Table 1.

The total drag coefficient and the average Nusselt number at $\mathrm{Re} = 30$ and $\mathrm{Pr} = 1.0$ are reported in the literature[49] as 2.11 and 5.08. It can be concluded that a mesh system with $81 \times 81$ grid points generates reasonable grid independent results. The outer boundary radius should be adjusted according to the Reynolds number. It was found that for all Re higher than 10, the outer boundary can be located 10 radii away from the sphere center, while for the lower Re, a larger domain is required.

Local Nusselt distributions at three different Reynolds numbers in comparison with available results[9] for $\mathrm{Pr} = 0.71$ are plotted in Figure 2, where reasonable agreements can be observed. Other flow parameters such as the wake length and separation angle have been validated in our previous work[32] and they are not repeated here.

Since no previous work on the heat transfer characteristics of the slip flow over solid sphere exists in the literature known to the authors of the present paper, the only case that can serve as a validation for the numerical results in this concern is an analytical solution proposed in this study which is valid for the $\mathrm{Re} \to 0$ limit. This is explained in detail in the following section.

## Results and discussions

The results can be presented in terms of either Knudsen or Trostel number, and the other one can be determined from equation (8). In this study, however, the results are presented in terms of the Knudsen number. Reynolds, Prandtl, and Knudsen numbers govern the flow and temperature fields in the presence

**Table 1.** Grid study at Re = 30 and Pr = 1.0.

| Grid | $C_D$ | Nu | $C_D$ rel. err. vs. Clift et al.[49](%) | Nu rel. err. vs. Clift et al.[49] (%) |
|---|---|---|---|---|
| 41 × 41 | 1.91 | 4.50 | 7.0 | 11.4 |
| 51 × 51 | 2.04 | 4.65 | 3.2 | 8.46 |
| 61 × 61 | 2.09 | 4.90 | 0.6 | 3.54 |
| 71 × 71 | 2.12 | 4.96 | 0.6 | 2.36 |
| 81 × 81 | 2.13 | 4.99 | 0.6 | 1.77 |
| 121 × 121 | 2.13 | 5.00 | 0.6 | 1.57 |

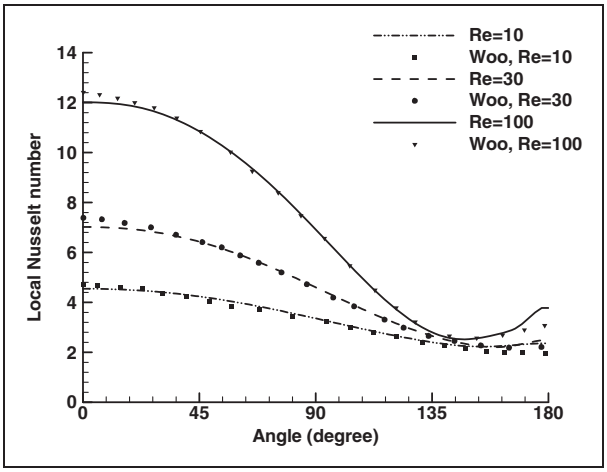


**Figure 2.** Surface Nusselt number comparison with the results of Woo[9] at Pr = 0.71.

of the velocity slip and temperature jump boundary conditions. In the present study, they are considered in the range of $0 \leqslant Re \leqslant 50$, $Kn \leqslant 0.1$ and $0.7 \leqslant Pr \leqslant 7.0$. The Pr numbers are selected according to the air and water Pr numbers at standard conditions that are Pr = 0.7 and 7, respectively. These values have been chosen based on the discussions performed on the two categories of slip flows. Air is a representative of gaseous slip flow due to the rarefaction effects and water is used for the liquid slippage over hydrophobic surfaces due to solid surface properties. The selection of the Re number has been performed according to the flow axisymmetric assumption. The onset of flow separation for flow over rigid sphere is $Re \approx 20$[49] and the onset of wake instability is $Re \approx 130$.[49] Therefore, it is preferred to keep a safe margin from this Re number to ensure that the axisymmetric condition is applicable.

In the following, slip effects on the flow and thermal wake structures, temperature jump distributions and local and average Nusselt numbers will be examined in detail.

Figure 3 shows the slip effects on the wake structure in the continuum and slip flow regimes at Re = 50 and Pr = 0.7. The sphere wake at this Reynolds number in the no-slip limit is rather large and slip effects can be more significant. This figure shows that as the Knudsen number increases, the wake length decreases considerably due to the slip velocity over the sphere surface, and it can be totally disappeared at higher Knudsen numbers.[32]

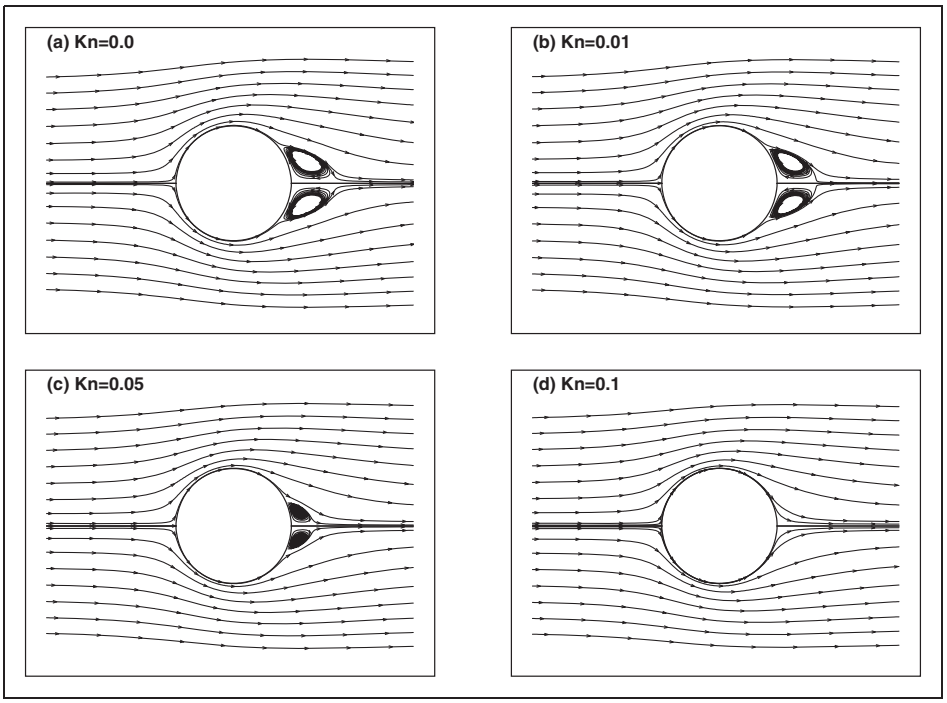


**Figure 3.** Slip effects on the sphere wake structure at Re = 50, Pr = 0.7, for (a) Kn = 0, (b) Kn = 0.01, (c) Kn = 0.05, and (d) Kn = 0.1.

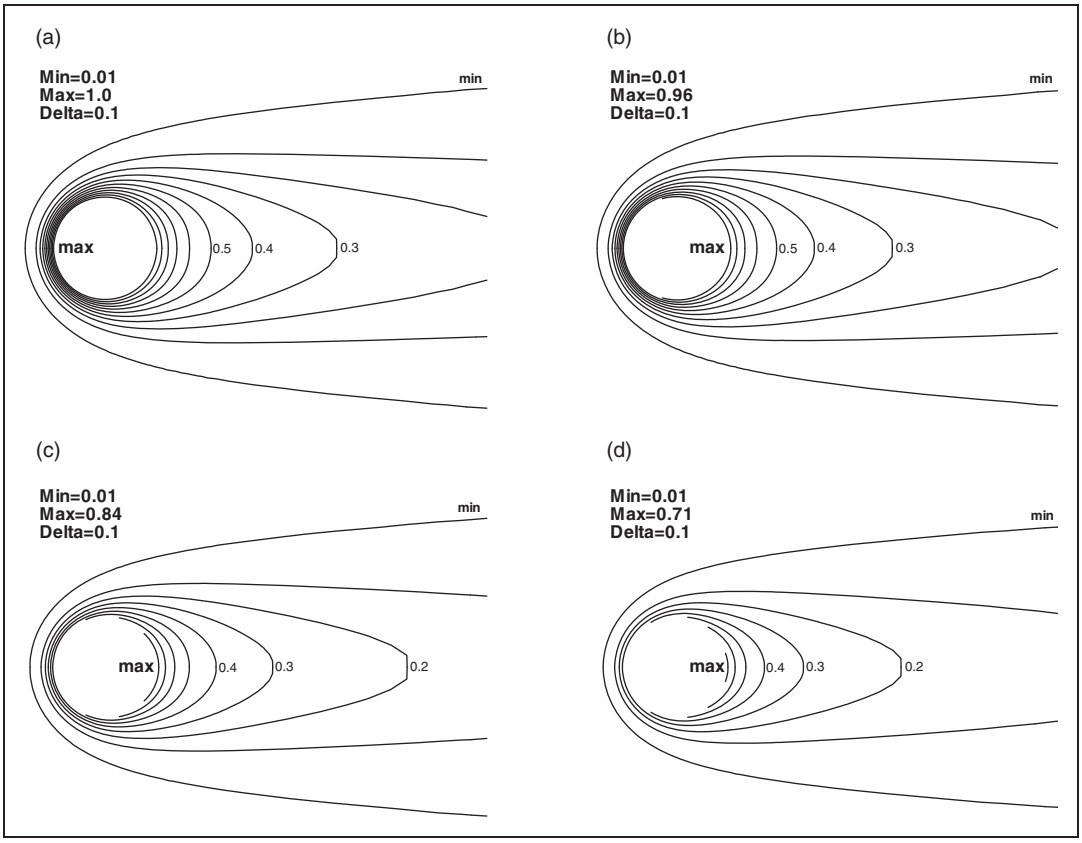


**Figure 4.** Temperature jump effects on the sphere non-dimensional temperature contour at Re = 50, Pr = 0.7, for (a) Kn = 0, (b) Kn = 0.01, (c) Kn = 0.05, and (d) Kn = 0.1.

Thermal wake structures in the continuum and slip flow regimes at the same Reynolds number and two Prandtl numbers of 0.7 and 7 are shown in Figures 4 and 5, respectively. In these figures, the contours of non-dimensional temperature defined as $\theta = (T - T_\infty)/(T_w - T_\infty)$ are plotted. Velocity slip and temperature jump have two opposing effects on the thermal wake region and the heat transfer rate. Temperature jump reduces the heat transfer rate because it decreases the temperature gradients in the gas layer adjacent to the wall and as a result, the thermal wake region shrinks as the Knudsen number increases. Conversely, the velocity slip increases the heat transfer rate due to the increase in convective effects near the wall where velocities are controlled by wall dragging effects. As a result, the thermal wake region grows as the Knudsen number increases. The relative importance of these two effects depends on the Knudsen and Prandtl numbers according to the equations (6) and (9) and also on the flow Reynolds number. As can be seen in Figure 4 for Pr = 0.7, the thermal wake region shrinks as the Knudsen number increases, while at Pr = 7.0, shown in Figure 5, the thermal wakes, which are thinner at all Knudsen numbers as expected for high Prandtl flows, slightly grow in the rear section by increasing the Knudsen number.

Furthermore, an interesting feature of the temperature field is that the maximum temperature occurs around the rear stagnation point since the maximum temperature jump is at the front stagnation point as shown in Figures 6 and 7. In these figures, temperature jump distributions over the solid sphere surface are plotted for varying Knudsen numbers at Re = 10 and Re = 50 for Pr = 0.7 and 7.0. The angle is measured from the front stagnation point. Temperature jump, $\theta_{jump}$, is defined as $\theta_{jump} = \theta_w - \theta_g$, where $\theta_w$ is the wall temperature and $\theta_g$ is the temperature of the gas layer adjacent to the wall. The figures show that the temperature jump values increase as the Knudsen number increases at both Reynolds numbers. The maximum temperature jump occurs at the front stagnation point due to the maximum temperature gradient at this point. As the Reynolds number increases, the surface temperature gradient increases resulting to higher values of the temperature jump.

In Figures 8 and 9, the local Nusselt number variations along the sphere surface at Re = 10 and Re = 50 for different values of Knudsen number are shown for both Pr = 0.7 and 7.0, respectively. The Nusselt number based on the sphere diameter, $D$, is defined as

$$Nu = \frac{hD}{k} = -\frac{D}{\Delta T_{ref}} \frac{\partial T}{\partial n} \tag{14}$$

where $\frac{\partial T}{\partial n}$ is the normal temperature gradient and $\Delta T_{ref} = T_w - T_\infty$.

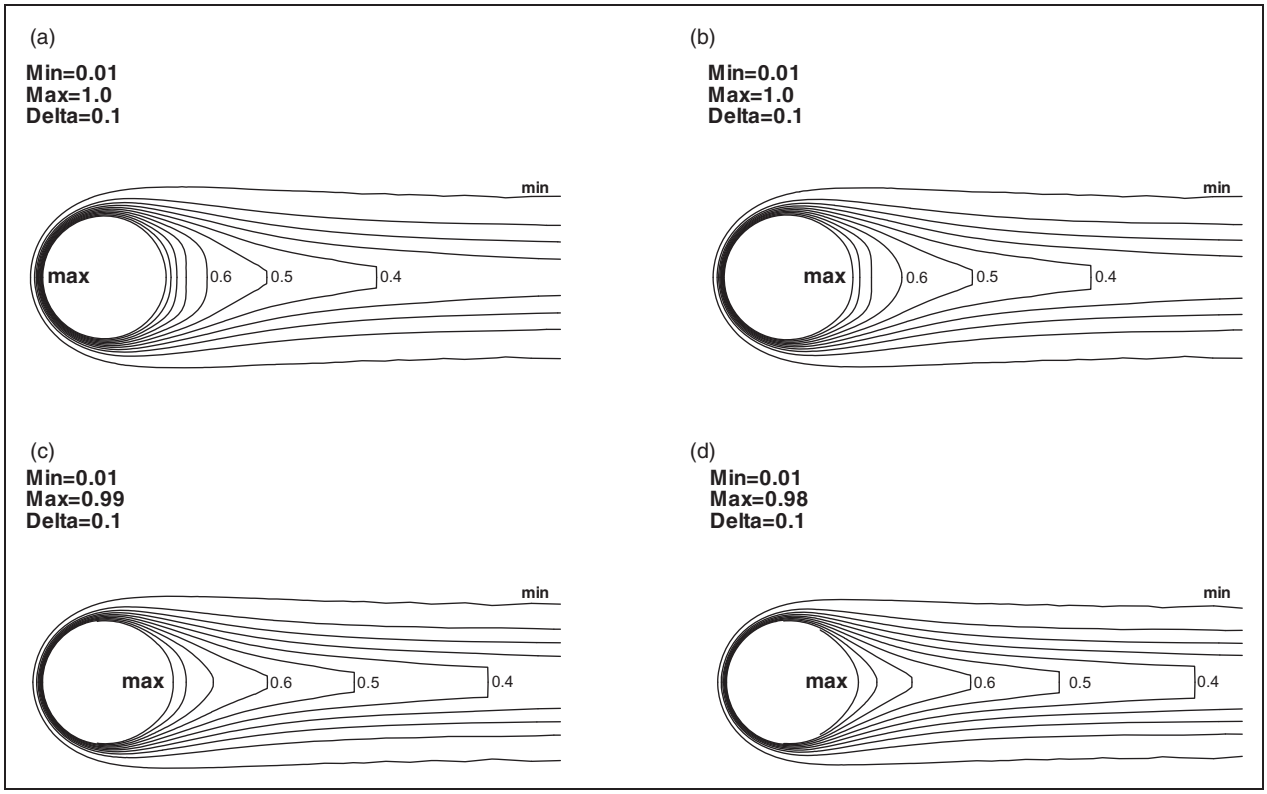


**Figure 5.** Temperature jump effects on the sphere non-dimensional temperature contour at Re = 50, Pr = 7.0, for (a) Kn = 0, (b) Kn = 0.01, (c) Kn = 0.05, and (d) Kn = 0.1.

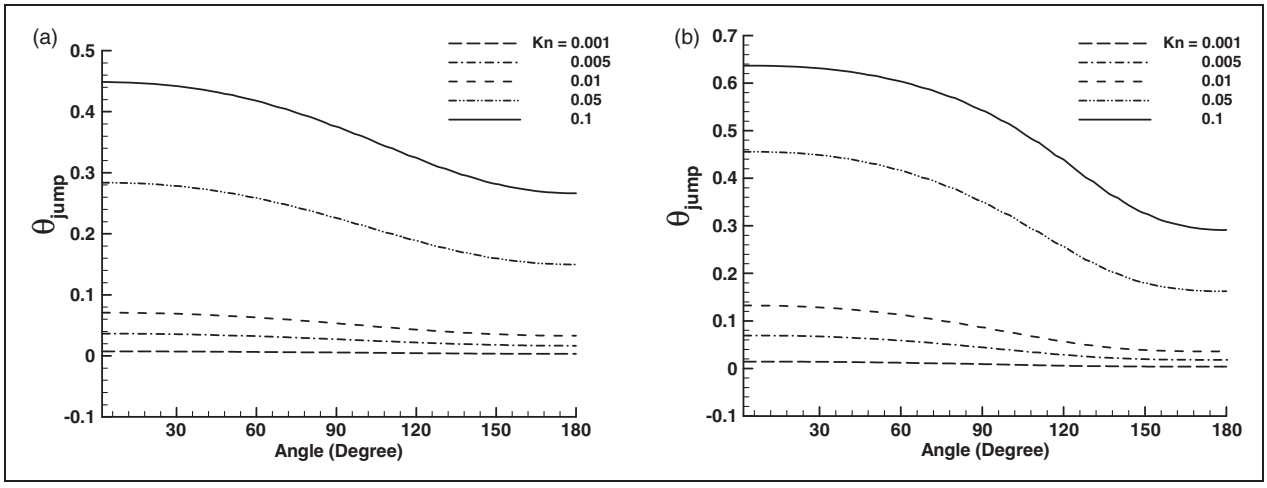


**Figure 6.** Temperature jump profiles at different Knudsen numbers for Pr = 0.7: (a) Re = 10 and (b) Re = 50.

The opposing effects mentioned above can be seen more clearly in the local distribution of the Nusselt number as shown in Figures 8 and 9 for different Prandtl and Knudsen numbers. As can be seen in Figure 8 which corresponds to Pr = 0.7, the maximum local Nusselt drop as compared to the no-slip case occurs at the front stagnation point, where the Nusselt number itself is maximum. In other words, for this Prandtl number the front stagnation point corresponds to the maximum temperature gradient, maximum Nusselt number and the maximum temperature jump point over the solid sphere surface. Moreover, as the Knudsen number increases, the Nusselt number decreases in both Reynolds numbers. It states that in this Prandtl number, the temperature jump effect is more dominant as compared to the velocity slip effect. While in Figure 9, which shows Nusselt distribution for Pr = 7.0, the temperature jump dominance on the heat transfer rate cannot be observed at all Knudsen numbers. As can be seen, the Knudsen effects on the local distribution of the Nusselt number are different in the front and the

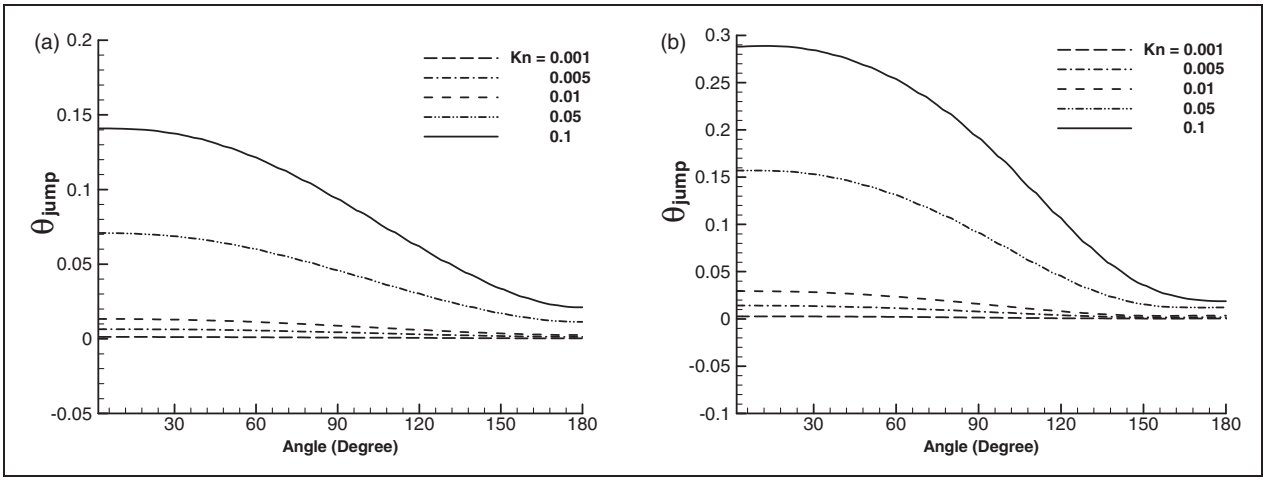


**Figure 7.** Temperature jump profiles at different Knudsen numbers for Pr = 7.0, (a) Re = 10 and (b) Re = 50.

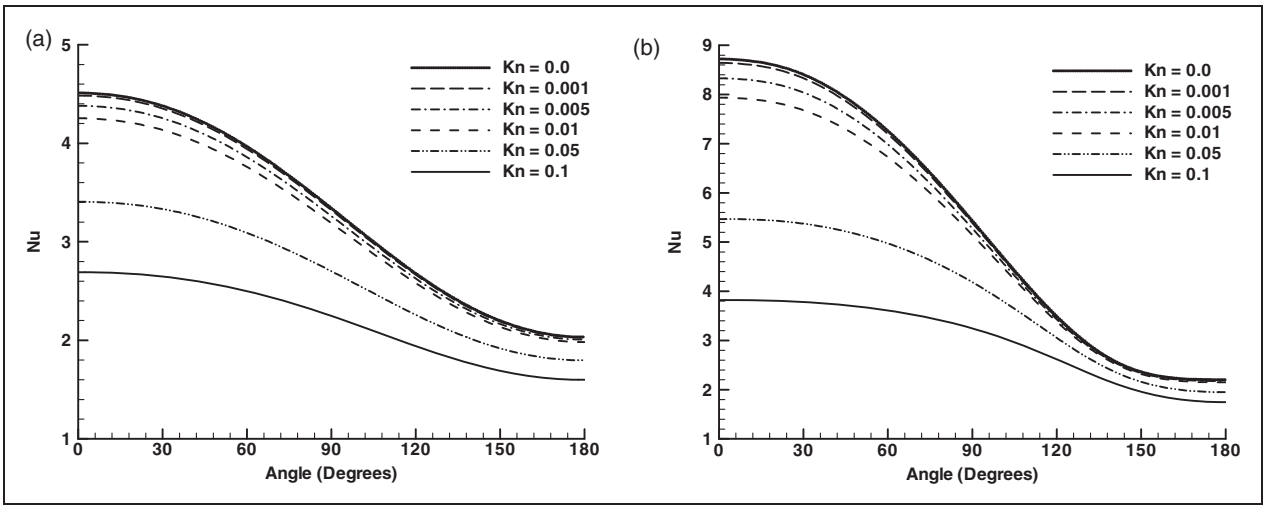


**Figure 8.** Nusselt distribution at different Knudsen numbers for Pr = 0.7: (a) Re = 10 and (b) Re = 50.

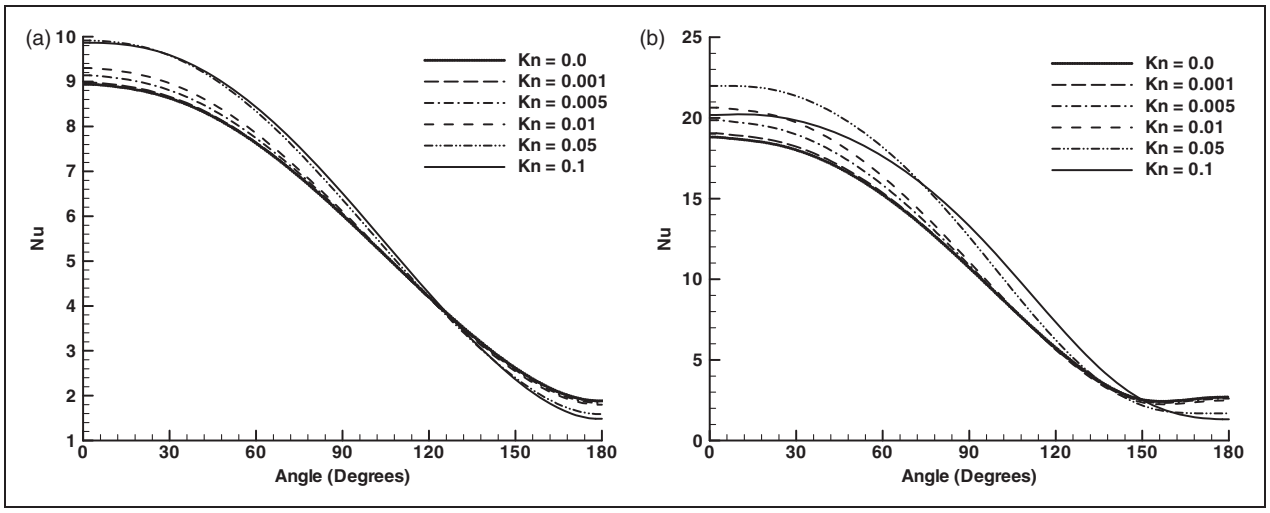


**Figure 9.** Nusselt distribution at different Knudsen numbers for Pr = 7.0: (a) Re = 10; (b) Re = 50.

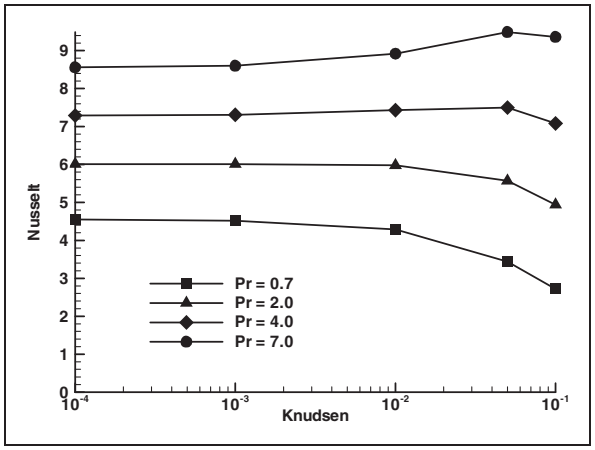


**Figure 10.** Effect of Prandtl number on the average Nusselt number variations as a function of Knudsen number, at Re = 30.

rear sections of the sphere. The increase of velocity slip is proportional to Knudsen number (equation 6) while the temperature jump increase is proportional to the Kn/Pr ratio (equation 9). Therefore, as the Prandtl number increases the relative importance of the temperature jump decreases, depending on the Reynolds number.

The effect of Prandtl number on the average Nusselt number is plotted in Figure 10 for varying Knudsen number at Re = 30. As the figure shows, at lower Prandtl numbers (Pr = 0.7 and 2.0), the Nusselt number decreases as the Knudsen number increases, due to the domination of the temperature jump effects over the slip velocity effects. However, at higher Prandtl numbers (Pr = 4.0 and 7.0), the Nusselt number initially increases as the Knudsen number increases indicating the dominance of the velocity slip effects, while at higher Knudsen numbers of about Kn = 0.05 the temperature jump effects gradually gains more weight over the velocity slip effects and prevents the increasing trend of the Nusselt number.

For the limiting case of $\mathrm{Re} \to 0$, one can find an analytical solution for the problem, which can also serve as a validation case for the presented numerical scheme. In this limit, the energy equation reduces to $\nabla^2 T = 0$, corresponding to the pure conduction around an isothermal solid sphere with temperature jump boundary condition. The fluid temperature distribution for this case reads to

$$T = -\frac{R^2(T_\infty - T_w)}{R + \frac{2\gamma}{\gamma+1}\frac{2-\sigma_T}{\sigma_T}\frac{\mathrm{Kn}\,D}{\mathrm{Pr}}}\frac{1}{r} + T_\infty \tag{15}$$

And the corresponding Nusselt number is

$$\mathrm{Nu} = \frac{1}{0.5 + \frac{2\gamma}{\gamma+1}\frac{2-\sigma_T}{\sigma_T}\frac{\mathrm{Kn}}{\mathrm{Pr}}} \tag{16}$$

At this limiting Reynolds number, for instance, the Nusselt number reduction due to the jump effects amounts to 25%, at Kn = 0.1, Pr = 0.7 for $\gamma = 1.4$ and $\sigma_T = 1$, while the reduction is only 3% at the same Kn and $\sigma_T$ for Pr = 7.0 and $\gamma = 1.0$. The numerical results also agree well with these analytical results.

## Conclusions

Heat transfer characteristics of slip flow over an isothermal impermeable solid sphere is investigated by solving the momentum and energy equations numerically with appropriate velocity slip and temperature jump boundary conditions in the range of $0 \leqslant \mathrm{Re} \leqslant 50$, $\mathrm{Kn} \leqslant 0.1$ and $0.7 \leqslant \mathrm{Pr} \leqslant 7.0$. The major findings of this study can be summarized as follows

- The wake region shrinks as the Knudsen number increases such that it can be completely disappeared at higher limits of the slip flow regime. This is due to the increase in the velocity slip on the solid sphere surface and the resultant increase in convective effects near the wall.
- The size of the thermal wake region according to the Knudsen number depends on the Prandtl number. At lower Prandtl numbers, the thermal wake region shrinks as the Knudsen number increases. Conversely, at higher Prandtl numbers, the higher the Knudsen number, the larger the thermal wake region.
- Temperature jump increases as the Reynolds and Knudsen numbers increase. The point associated with the maximum temperature jump is located at the front stagnation point.
- The average Nusselt number variation with the Knudsen number depends on the Prandtl and Reynolds numbers. For an intermediate Reynolds number of 30, the Nusselt number decreases as the Knudsen number increase at low Prandtl numbers ($0.7 \leqslant \mathrm{Pr} \leqslant 2.0$), while at higher Prandtl numbers, a non-linear trend is observed.
- For the limiting case of $\mathrm{Re} \to 0$, an analytical solution for predicting the average Nusselt number in the slip flow regime is developed which served as a validation case for the numerical simulations.

### Declaration of Conflicting Interests

The author(s) declared no potential conflicts of interest with respect to the research, authorship, and/or publication of this article.

### Funding

The author(s) received no financial support for the research, authorship, and/or publication of this article.

### References

1. Stokes GG. *On the effect of the internal friction of fluids on the motion of pendulums mathematical and physical papers*. Cambridge: Cambridge University Press, 2009.

2. Tomotika S and Aoi T. The steady flow of viscous fluid past a sphere and circular cylinder at small Reynolds numbers. *Q J Mech Appl Math* 1950; 3: 141–161.
3. Hadamard JS. Mouvement permanent lent d'une sphere liquide et visqueuse dans un liquide visqueux. *Comptes Rendus de l'Académie des Sci* 1911; 152: 1735–1738.
4. Rybczynski W. Über die fortschreitende Bewegung einer flüssigen Kugel in einem zähen Medium. *Bulletin International de Academie des Sciences de Cracovie* 1911; 40: 40–46.
5. LeClair BP. *Viscous flow in multi particle systems at intermediate Reynolds numbers*. Hamilton, ON: McMaster University, 1970.
6. Le Clair BP, Hamielec AE and Pruppacher HR. A numerical study of the drag on a sphere at low and intermediate Reynolds numbers. *J Atmos Sci* 1970; 27: 308–315.
7. Masliyah JH. *Symmetric flow past orthotropic bodies: single and clusters*. Vancouver: University of British Columbia, 1970.
8. Ihme F, Schmidt-Traub H and Brauer H. Theoretical studies on mass transfer and flow past spheres. *Chemie Ingenieur Technik* 1972; 44: 306–313.
9. Woo SW. *Simultaneous free and forced convection around submerged cylinders and spheres*. Hamilton, ON: McMaster University, 1971.
10. Taneda S. Experimental investigation of the wake behind a sphere at low Reynolds numbers. *J Phys Soc Japan* 1956; 11: 1104–1108.
11. Seeley LE. *An experimental investigation of laminar and turbulent flow around a sphere at intermediate Reynolds numbers*. Toronto, Ontario: University of Toronto, 1972.
12. Roshko A. Transition in incompressible near-wakes. *J Phys Fluid* 1967; 10: 5181–5183.
13. Roshko A. Experiments on the flow past a circular cylinder at very high Reynolds number. *J Fluid Mech* 1961; 10: 345–356.
14. Carslaw HS and Jaeger JC. *Conduction of heat in solids*. Oxford: Oxford University Press, 1947.
15. Feng ZG and Michaelides EE. Unsteady heat transfer from a spherical particle at Finite Peclet numbers. *J Phys Fluid* 1996; 118: 96–102.
16. Al-Taha TR. *A numerical solution of Navier–Stokes and energy equations for heat transfer from particles*. London: Imperial College, 1969.
17. Dennis SCR, Walker JDA and Hudson JD. Heat transfer from a sphere at low Reynolds numbers. *J Fluid Mech* 1973; 60: 273–283.
18. Hatim JD. *Theoretical study of heat transfer from a solid sphere accelerating from rest*. London, United Kingdom: London University, 1975.
19. Masliyah JH and Epstein N. Numerical solution of heat and mass transfer from spheroids in steady axisymmetric flow. *Progr Heat Mass Transf* 1972; 6: 613–632.
20. Karniadakis G, Beskok A and Aluru N. *Microflows and nanoflows, fundamentals and simulation*. New York, USA: Springer, 2005.
21. Watanabe K, Udagawa Y and Udagawa H. Drag reduction of Newtonian fluid in a circular pipe with a highly water-repellent wall. *J Fluid Mech* 1999; 381: 225–238.
22. Pitcher G, Wigley G and Saffman M. Velocity and drop size measurements in fuel sprays in a direct injection diesel engine. *Particle Particle Syst Characteriz* 1990; 7: 160–168.
23. Fletcher DF, Guo B, Harvie DJE, et al. What is important in the simulation of spray dryer performance and how do current CFD models perform? *Appl Math Model* 2006; 30: 1281–1292.
24. Cunningham E. On the velocity of steady fall of spherical particles through fluid medium. Proc Royal Soc London A 1910; 83: 357–365.
25. Millikan RA. The isolation of an ion, a precision measurement of its charge, and the correction of Stokes's lawPhys Rev (Series I) 1911; 32: 349–397.
26. Knudsen M and Weber S. Air resistance for the slow motion of small spheres. *Ann Phys* 1911; 36: 981–994.
27. Millikan RA. The general law of fall of a small spherical body through a gas and its bearing upon the nature of molecular reflection from surfaces. Phys Rev (Series I) 1923; 22: 1–23.
28. Allen MD and Raabe OG. Slip correction measurements of spherical solid aerosol particles in an improved millikan apparatus. *Aerosol Sci Technol* 1985; 4: 269–286.
29. Rader DJ. Momentum slip correction factor for small particles in nine common gases. *J Aerosol Sci* 1990; 21: 161–168.
30. Kim JH, Mulholland GW, Kukuck SR, et al. Slip correction measurements of certified PSL nanoparticles using a nanometer differential mobility analyzer (nano-DMA) for Knudsen Number From 0.5 to 83. *J Res Natl Instit Standard Technol* 2005; 110: 31–54.
31. Moshfegh A, Shams M, Ahmadi G, et al. A novel surface-slip correction for microparticles motion. *Colloid Surface A: Physicochem Eng Aspects* 2009; 345: 112–120.
32. Niazmand H and Anbarsooz M. Slip flow over micron-sized spherical particles at intermediate Reynolds numbers. *J Mech Sci Technol* 2012; 26: 2741–2749.
33. Moshfegh A, Shams M, Ahmadi G, et al. A new expression for spherical aerosol drag in slip flow regime. *J Aerosol Sci* 2010; 41: 384–400.
34. Shokouhmand H and Bigham S. Slip-flow and heat transfer of gaseous flows in the entrance of a wavy microchannel. *Int Commun Heat Mass Transf* 2010; 37: 695–702.
35. Shokouhmand H, Bigham S and Nasr Isfahani R. Effects of Knudsen number and geometry on gaseous flow and heat transfer in a constricted microchannel. *Heat Mass Transf* 2011; 47: 119–130.
36. Bigham S, Hossein Shokouhmand H, Isfahani RN, et al. Fluid flow and heat transfer simulation in a constricted microchannel: effects of rarefaction, geometry, and viscous dissipation. *Num Heat Transf, Part A: Appl: Int J Computat Methodol* 2011; 59: 209–230.
37. Sui Y, Teo CJ, Lee PS, et al. Fluid flow and heat transfer in wavy microchannels. *Int J Heat Mass Transf* 2010; 53: 2760–2772.
38. Atefi GH, Niazmand H and Meigounpoory MR. Numerical analysis of 3-D flow past a stationary sphere with slip condition at low and moderate Reynolds numbers. *J Dispers Sci Technol* 2007; 28: 591–602.
39. Watanabe K, Okido K and Mizunuma H. Drag reduction in flow through square and rectangular ducts with highly water-repellent walls. *Transact Japan Soc Mech Eng Series B* 1996; 62: 3330–3334.

40. Watanabe K and Ogata S. Drag reduction for a rotating disk with highly water-repellent wall. *JSME Int J Ser B* 1998; 41: 556–560.
41. Watanabe K, Yanuar and Mizunuma H. Slip of Netwonian fluids at slid boundary. *JSME Int J Ser B* 1998; 41: 525–529.
42. Niazmand H. *Numerical study of thermocappilary effects on transient droplet heating and vaporization*. Davis: University of California, 1993.
43. Dwyer HA. Calculations of droplet dynamics in high temperature environments. *Progr Energy Combust Sci* 1989; 15: 131–158.
44. Maxwell JC. On stresses in rarified gases arising from inequalities of temperature. *Philos Transact Royal Soc London* 1879; 170: 231–256.
45. Trostel R. Gedanken zur Konstruktion mechanischer Theorien II. Forschungsbericht, No. 7, 2. Technical University of Berlin. 1988.
46. Smoluchowski von Smolan M. Ueber Wärmeleitung in verdünnten Gasen. *Annalen der Physik* 1898; 300: 101–130.
47. Chorin AJ. Numerical solution of the Navier–Stokes equations. *Math Computat* 1968; 22: 745–762.
48. Niazmand H, Renksizbulut M and Saeedi E. Developing slip-flow and heat transfer in trapezoidal microchannels. *Int J Heat Mass Transf* 2008; 51: 6126–6135.
49. Clift R, Grace JR and Weber ME. *Bubbles, drops, and particles*. New York: Academic Press, 1978.